Extended Study on Electrophoretic Deposition Process of Inorganic Octahedral Metal Clusters: Advanced Multifunctional Transparent Nanocomposite Thin Films

Ngan T. K. Nguyen,[1,2] **Adèle Renaud,**[3] **Benjamin Dierre,**[1,2] **Barbara Bouteille,**[1,2] **Maxence Wilmet,**[1,3] **Marion Dubernet,**[1,2] **Naoki Ohashi,**[1,2] **Fabien Grasset,**[*1,2] **and Tetsuo Uchikoshi**[*1,2]

[1]CNRS - Saint-Gobain - NIMS, UMI3629, Laboratory for Innovative Key Materials and Structures (LINK), National Institute for Materials Science, 1-1 Namiki, Tsukuba, Ibaraki 305-0044, Japan

[2]National Institute for Materials Science (NIMS), Research Center for Functional Materials (RCFM), 1-1 Namiki, Tsukuba, Ibaraki 305-0044, Japan

[3]Univ Rennes, CNRS, ISCR-UMR 6226, F-35000 Rennes, France

E-mail: fabien.grasset@univ-rennes1.fr (F. Grasset), UCHIKOSHI.Tetsuo@nims.go.jp (T. Uchikoshi)

Fabien Grasset
Dr. Fabien Grasset received his Ph. D. degree in 1998 from the University of Bordeaux I in the field of solid state chemistry and material science at the ICMCB laboratory. In 2000–2001, he was a post-doc researcher at NIMS and widened his research to nanomaterials and colloidal science. After 13 years' experience as associate professor at the University of Rennes 1, he joined the CNRS as Director of Research in 2014. He is currently Co-Director of the LINK project, a joint international laboratory between NIMS, Saint-Gobain and CNRS based in Tsukuba, Japan.

Tetsuo Uchikoshi
Dr. Tetsuo Uchikoshi is a group leader and a co-director of the LINK Center at NIMS, a visiting professor at Hokkaido University and a part-time lecturer at Hosei University. He received his B.S. in metallurgical engineering (in 1986) and Ph.D. in Materials Science (in 1994) from Waseda University. He joined the National Research Institute for Metals (NRIM), the predecessor of NIMS, as a researcher. After spending years as a senior researcher, a principal researcher, and a chief researcher, he has been a group leader of the Fine Particles Engineering Group at NIMS since 2011. He worked as a visiting researcher under the guidance of Prof. P. S. Nicholson at McMaster University in Canada in 1997–1998 and a visiting professor at Kumamoto University in 2009–2012. He has held the title of Fellow of the Ceramics Society of Japan since 2016.

Abstract

This review paper summarizes our very recent works on the synthesis of multifunctional transparent nanocomposite thin films or coatings based on metal atom clusters by an electrophoretic deposition (EPD) process. Eight different octahedral atom clusters with niobium, molybdenum or tantalum as metallic cores were used to prepare highly transparent thin films in the visible. Green, yellow, orange, red and brown colored films were successfully fabricated by coating on a transparent conductive oxide glass substrate. Transparent nanocomposite films with prominent luminescent properties were obtained by using Mo_6 clusters whereas ultra-violet (UV) and near infrared (NIR) filters were realized by using Nb_6 or Ta_6 clusters. The EPD process appears to be a new strategy to fabricate highly trans-parent, homogeneous and colored nanocomposite thin films and coatings for smart windows and solar technologies in a very short time ($<90\,s$).

1. Introduction

Thin films or coatings, with thickness ranging from nano-meters to a few tens of micrometers are playing a very impor-tant and indispensable role in daily life with a material market value estimated to be around $11 billion for 2018 for end-user industries.[1] Photovoltaic solar cells, microelectromechanical or

electrical systems, semiconductors, sensors, anticorrosion and optical coatings are the main applications of thin film technology. Several kinds of devices, including organic and/or inorganic nanomaterials, have been developed so far in order to respond to some of these applications.[2–6] Recently, the demand for new, robust, low cost and environmentally-friendly transparent functional thin films for window applications is strongly increasing. The main application for these functional coatings with high transparency in the visible are self-cleaning,[7] photovoltaic[8,9] or solar control materials.[10–14] These demands are spurring the design of transparent nanomaterials that exhibit engineered physical properties and that can enable fabrication methods for low cost, low waste, large area and even flexible devices. The thin films are generally fabricated by physical vapor deposition (sputtering, evaporation, laser ablation, etc.), chemical vapor deposition (atomic layer deposition, etc.) or chemical solution deposition (sol-gel, electrophoretic deposition (EPD), etc.) processes. In recent years, the use of solution processes is highly desirable in order to reduce cost and waste. In this way, the EPD process has been challenged by the development of nanomaterials and processes that allow bottom up fabrication.[15–28]

Since the establishment of the international joint research unit in 2014 between NIMS, Saint-Gobain and CNRS, called Laboratory for Innovative Key Materials and Structures (LINK),[29] we focused on the development of a new strategy using an EPD process to fabricate highly transparent and colored nanocomposite thin films and coatings for smart windows and solar technologies based on inorganic transition metal atom clusters. EPD offers great combinations of cost effectiveness, long-range consistency in film thickness and surface morphology, size-scalability, high deposition rates, and site-selectivity. Indeed, in the general perspective of energy saving due to the increase in consumption and serious environmental problems induced by global warming, the realization of low-cost, low-waste and low-toxic selective coatings is a field of research of growing interest, especially as new phosphors or ultra-violet (UV) and near-infrared (NIR) barriers with a high visible transparency. In this context, we recently demonstrated the first integration of niobium, molybdenum or tantalum octahedral metal atom cluster compounds in multifunctional nanocomposite thin films for windows and solar technologies by using low and medium voltage EPD processes.[13,30–33] This technique seems to be very promising for preparing new thin film materials and this review gives a general survey of our recent works.

2. Experimental

Metal Cluster Powders. We have investigated eight compounds in two different well-known metal cluster families:
1) the $[Mo_6L^i_8L^a_6]^{2-}$ series (L^i = Cl, Br, I; L^a = Cl, Br, I, $OOCC_2F_5$) – namely $Cs_2Mo_6Cl_{14}$ (**1**), $Cs_2Mo_6Br_{14}$ (**2**), $Cs_2Mo_6I_{14}$ (**3**), $Cs_2Mo_6I_8(OOCC_2F_5)_6$ (**4**), and $((n-C_4H_9)_4N)_2$-Mo_6Br_{14} (**5**) 2) the $[M_6L^i_{12}L^a_6]^{n\pm}$ series (M = Nb, Ta; L^i = Cl, Br; L^a = Cl, Br, H_2O; $-4 < n < 2$) – namely $K_4Nb_6Cl_{18}$ (**6**), $K_4Nb_6Br_{18}$ (**7**) and $[Ta_6Br_{14}(H_2O)_4]3H_2O$ (**8**).

All the metal cluster powders were synthesized at the University of Rennes 1 (UMR 6226 UR1-CNRS). The compounds were synthesized according to procedures reported in
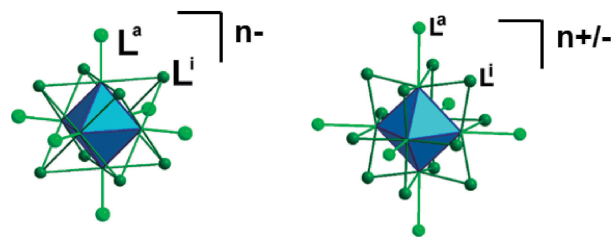

Figure 1. Structural view of octahedral $[M_6L^i_8L^a_6]^{n-}$ (left) and $[M_6L^i_{12}L^a_6]^{n\pm}$ (right) clusters.

the literature[34–39] and their schematic structural view is shown in Figure 1.

Preparation of the Metal Cluster Solutions. First, the as-synthesized powders of cluster compounds were dissolved in different solvents in order to determine the best conditions for EPD deposition. Distilled water, ethanol, 1-propanol, acetone, methyl ethyl ketone (MEK) or acetyl acetone solutions at the concentration of 5 g per liter were prepared. Reagent grade chemicals, distilled water (Water Purifier WG710, conductance of 0.5×10^{-4} S.m^{-1} at 25 °C), acetone (99.5%), MEK (99%), acetyl acetone (99%), 1-propanol (99.5%) and ethanol (99.5%), were used as received. All the solutions were magnetically stirred for fixed duration depending on the solvent. In the case of acetone or MEK, adding a small amount of water (0.15 to 0.5 mL) was necessary to improve the solubility of Nb$_6$ and Ta$_6$ clusters (**6**, **7** and **8**) and also to keep the green color of the Ta$_6$ cluster (**8**) in solution. For clusters **2**, a transparent solution was obtained in ethanol by addition of a small amount of water. Except for clusters **2**, **3** and **5**, a polymer should be added as binders in order to obtain highly transparent thin films by EPD. Poly(vinylpyrrolidone) (PVP, molecular weight (Mw) = 40 000 g.mol^{-1}), cellulose acetate phthalate (CAP, Mw = 2534 g.mol^{-1}) and poly(methylmethacrylate) (PMMA, Mw = 350 000 g.mol^{-1}) gave the best results and were used as received without any purification.

Fabrication of the Thin Films by EPD. Before application of the EPD process, the indium tin oxide (ITO) glass substrates were washed with detergent and distilled water then acetone for 30 minutes by sonication. ITO glass substrates (Geomatec Co., Ltd (Japan), 6–8 Ohm sq^{-1}) were connected to a Keithley Model 2400 Series SourceMeter as the anodic (or cathodic) substrate and as the counter electrode (Figure 2). Voltages from 5 to 50 V and deposition times from 10 to 90 s were applied. EPD experiments were conducted using each of these solutions after a filtration process (0.2 mm). The deposition area of the ITO glass was approximately 2 cm^2 (1 × 2 cm) or 20 cm^2 (4 × 5 cm). The applied voltages and deposition time of the EPD were separately optimized for each solvent and metal cluster. The deposit weight was determined by subtracting the weight of the ITO glass before and after EPD. The prepared thin films were slowly dried in air and used for characterization of the properties.

Characterization Methods. The zeta potential and conductivity of the cluster solutions were measured with a zeta-potential analyzer (Malvern Instrument, Ltd., Zetasizer Nano Z: zeta potential-measurable particle size is 5 nm–10 μm). The particle sizes in solution were measured by a dynamic light scattering (DLS) technique using a Nano Q V2.5.9.0 analyzer
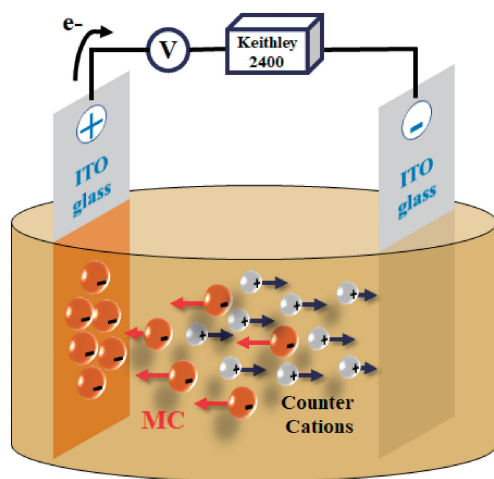
Figure 2. Schematic diagram showing the experimental setup for anodic EPD of octahedral metal clusters.

(Cordouan Technologies) at the wavelength of 657 nm. A high resolution-color 3D laser microscope with a 408 nm laser was used for the measurement of the thickness of the films formed at different deposition times.

The chemical composition was analyzed by coupling several techniques, such as Fourier transform infrared spectroscopy (FTIR) (Thermoscientific Nicolet 4700) in the wavenumber range from 4000 to 400 cm^{-1} and X-ray fluorescence (XRF) (EZX Primus II, Rigaku). X-ray photoelectron spectrometry (XPS) spectra were measured with a PHI Quantera SXM (ULVAC-PHI) using Al Kα radiation at 20 kV and 5 mA, neutralization by Ar^+, pass energy of 55 eV and the take-off angle of 45°. The Raman scattering spectra were measured using a LabRam high resolution spectrometer coupled to a confocal microscope (Horiba Yobin Yvon), with 600 g/mm grating and 10 × objective. A He-Ne 633 nm laser was used for the scattering excitation. The Raman spectra were recorded at room temperature with a 100 s exposure and 2 accumulations.

The microstructure of the thin films was studied by several complementary techniques. For instance, X-ray diffraction measurements (XRD) were performed with a Rigaku Ultima 3 Rint 2000 diffractometer at 40 kV, 30 mA in the 2θ angle range from 5° to 50° with Cu Kα radiation (λ = 1.54 Å). Field emission-scanning electron microscopy (FE-SEM) images were obtained using a JEOL JSM 6301F microscope operating at 7 kV. Scanning transmission electron microscopy (STEM) images of the films were taken using a Cs-corrected JEOL JEM2100F microscope operating at 200 kV. It is equipped with a field-emission electron gun and incorporates multiple additional functions (energy-dispersive spectrometer (EDX) and a high sensitivity Z-contrast high angular annular dark field (HAADF)).

The optical absorbance of the solutions and transmission of the films were measured with a UV-Vis-NIR spectroscopy (Jasco V570) in the wavelength range of 220 nm to 2000 nm at the scan rate of 400 nm/s. The emission spectra of the cluster films were obtained by high performance fluorescence spectroscopy (FL) (FP8500, Jasco Corp.) connected to a xenon lamp at the scan rate of 500 nm/s. In some cases, a microphotoluminescence (PL) system (LabRam HR, Horiba Corp.) with a 325-nm He-Cd laser system was used to record the emission peak in the wavelength range of 350 nm and 1000 nm.

3. Results and Discussion

General Description of EPD. The EPD process, i.e. moving of particles under an electric field, has been known for more than two centuries.[40] The theoretical aspects of this process were first studied by Hamaker and Verwey in 1940,[41] but it received attention in the field of advanced ceramics only in the 1980s. Nowadays, EPD is one of the most promising electrochemical methods to prepare coatings because of its simple setup (Figure 2); room temperature, ambient pressure, short process time and easy control of the film thickness. Deposition is generally described by a two-step process. It occurs when electric-field driven colloidal particles suspended in a fluid migrate toward an electrode (step 1) where they assemble or coagulate into a deposit (step 2). There are a lot of factors influencing EPD, and most of them are inter-related. They have to be carefully controlled to optimize the process. The deposition depends on many parameters, such as the solvent (viscosity, dielectric constant), the particle size, the volume fraction of colloids, the use of binders, the applied field strength and time, and the electrophoretic mobility. The latter is dependent on the ionic strength, permittivity, and viscosity of the solution as well as the electric potential difference between the surface of the colloid and suspension (termed the zeta-potential). Since its discovery, many experiments involving a large variety of materials have been performed to optimize the parameters and investigate the deposition mechanisms occurring during the EPD process.[42–50] Fundamental studies to fabricate thin films of hydroxyapatite,[51,52] SiO_2,[53] carbon nanotubes,[54–56] graphene,[57] Al_2O_3,[58] TiO_2,[59–61] ZnO,[62,63] forsterite,[64] metal-organic frameworks (MOFs),[65,66] ligand-covered metal particles[67] and a fluorescent Cu or Au sheet for light-emitting diodes,[68] have been performed by EPD.

General Description of Metal Cluster Units. In the past decades, transition metal cluster compounds have shown interesting and rich complexity of structural and physical/chemical properties.[69,70] Solid state compounds have some specific electronic and electrochemical properties with strong potential for energy storage and supply applications (superconductivity, batteries, thermoelectricity, hydrogen affinity, etc.).[71–76] Moreover, their good solubility in various solvents provides a wide range of processing routes to elaborate molecular assemblies and nanocomposite materials.[77] Thus, very recently, a large variety of M-based metal cluster nanocomposites (M = Nb, Mo, Ta) have been investigated for potential applications in optics,[13,30–33,78–82] solar cells,[83–85] photocatalysis,[86–90] and biotechnologies.[91–107] Additionally, their high chemical flexibility has already allowed the fabrication of transparent nanocomposite thin films in organic or inorganic matrices that can be easily coated on substrates for photonic applications.[13,30–33,108–110]

New Nanocomposite Thin Films Based on Mo₆ Cluster for Optical Applications. All Inorganic Mo₆ (2, 3 and 5) Coatings:

Morphology and Structure; From all the tested solvents, MEK was evidenced as the best solvent to obtain transparent and crack-free thin films[30–32] (Figure 3a). The zeta potential of solutions showed negative values (2: −21 ± 1.2;
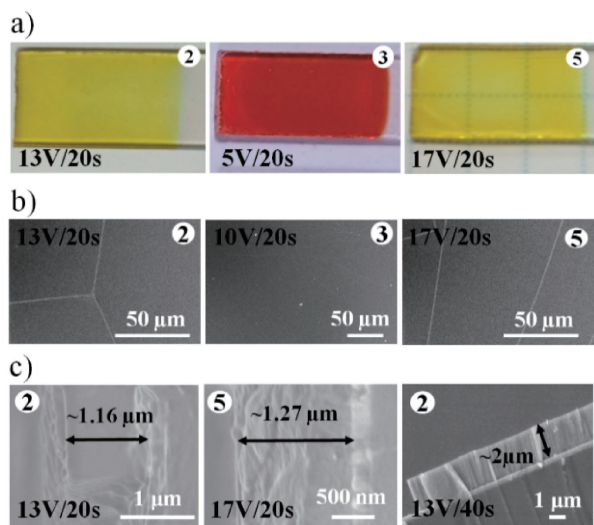
Figure 3. a) The photographs (size of ITO glass is 1×2 cm), b) homogeneous morphology, and c) the cross section image of the deposit films based on **2**, **3** and **5** cluster.

Table 1. Best deposition parameters for Mo_6 clusters in MEK solution

	Deposition time (s)	Applied voltage (V)	Concentration (g/L)	Electric conductivity (mS/cm)
Cluster **2**	30	13	5	0.33 ± 0.01
Cluster **3**	30	5	5	0.20 ± 0.01
Cluster **5**	30	17	5	0.30 ± 0.03

3: -11.8 ± 0.8; **5**: -26.4 ± 1.7) due to the existence of $[Mo_6X_{14}]^{2-}$ units (X = Br, I) in the solution. These negative values of the zeta potential are fully consistent with the negative charge of the clusters and allowed us to perform anodic EPD. The values of the conductivity were measured between 0.4 and 0.2 mS/cm. The best deposition parameters are reported in Table 1. Figure 3a shows the films obtained from the different solutions under visible light. Yellow and red thin films were obtained from Br or I ligands respectively. This result is in perfect agreement with the absorption spectra of clusters **2** and **3**.[94] We noticed that it is possible to easily tune the absorption by changing the deposition time (30 s to 120 s), the applied voltage (3 to 20 V) or the solution concentration (1 to 5 g/L) in the case of the cluster **3**. In all cases, the surfaces of the thin films showed smooth and homogeneous morphology (Figure 3b). The thickness of about 1 μm was attained in the first 10 s and it increased to a maximum of 2 μm when the deposition time exceed 40 s (Figure 3c).

We particularly focused on the microstructural characterization of the films prepared with clusters **2** and **5**. The XRD patterns of the film samples presented a broad peak at the 2θ angle of 11° suggesting a low crystallinity of the films deposited by EPD. This broad peak assigned to randomly deposited nanosize octahedral Mo_6 cluster units, which gives this amorphous-like peak. This result was confirmed by HRTEM analysis which indicated that the sample consisted of an amorphous phase mixing with crystallized nanoparticles (average
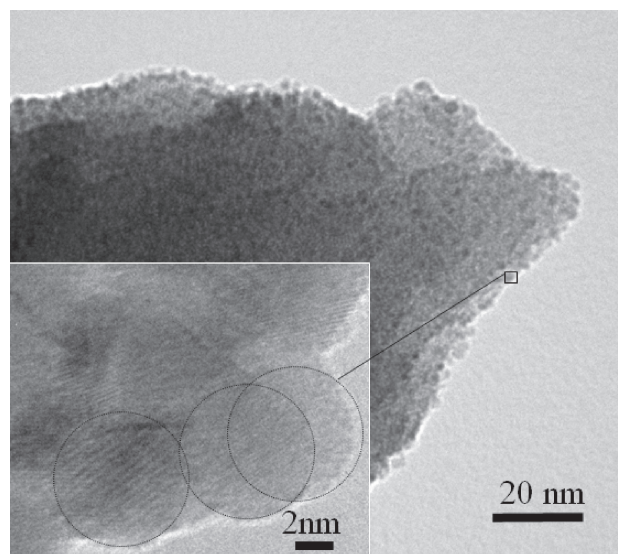

Figure 4. The distribution of the Mo_6 nanoparticle near the substrate surface estimated by HRTEM images.

diameter lower than 6 nm) quite homogeneously distributed only near the substrate (Figure 4). In parallel, the chemical composition and structure of the film were clearly characterized by using complementary techniques like XRF, TEM-EDX, STEM and XPS.[31] The EDX-TEM mapping shown homogeneous distribution of Br and Mo atoms in contrast to that of Cs atoms, which was not significantly measured (Figure 5a). The disappearance of Cs^+ cations was also confirmed by XRF and XPS analyses and is mainly explained by the positive charge and the attraction to the cathode instead of the anode electrode. XPS analysis of cluster **2** in powder form or after EPD deposition are represented on Figure 5b. XPS investigation also indicated that on average each primary octahedral $[Mo_6Br^i_8-Br^a_6]^{2-}$ cluster unit deposited in the film lost 2 apical Br atoms, which are replaced by two OH^- groups or H_2O molecules originated from the solvent to form either $[Mo_6Br^i_8Br^a_{6-x}-(OH)^a_x]^{2-}$ or $[Mo_6Br^i_8Br^a_4(H_2O)^a_2]$ cluster units. Both of them are known to exhibit a stable octahedral structure.[111,112] This model was recently supported by time of flight mass spectrometry (TOF-MS) experiments realized in collaboration with Institut Lumière Matière (ILM) in Lyon [not shown].

Though the deposition process seemed to be fairly good, the Mo_6 films were sometimes cracked within a short time during the evaporation of the solvent or even after a couple of days. In order to improve the interaction between the Mo_6 film and the ITO surface, a hydrophilic plasma treatment of the ITO surface was first performed by plasma ion bombardment (PIB-10) (discharge current of 10 mV and processing time of 3 minutes). The hydrophilized ITO glasses showed much better adhesion of the Mo_6 film after the EPD, but the film still cracked after a few weeks. Considering the advantages of polydimethylsiloxance (PDMS) in coating application areas, a PDMS coating was carried out as a post-treatment. PDMS with a viscosity of 1.5 and 2 centistocks were used as top coatings on the surface of the Mo_6 octahedral cluster films after EPD. This additional top layer clearly improved the mechanical properties by limitation of the hairline cracks without changing the homogeneity or
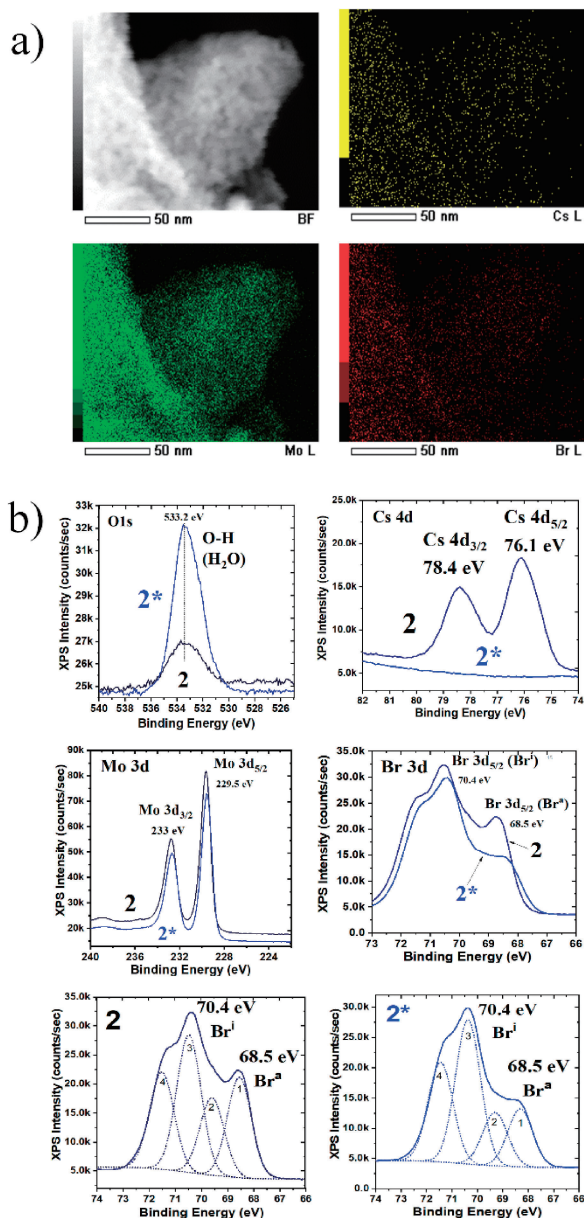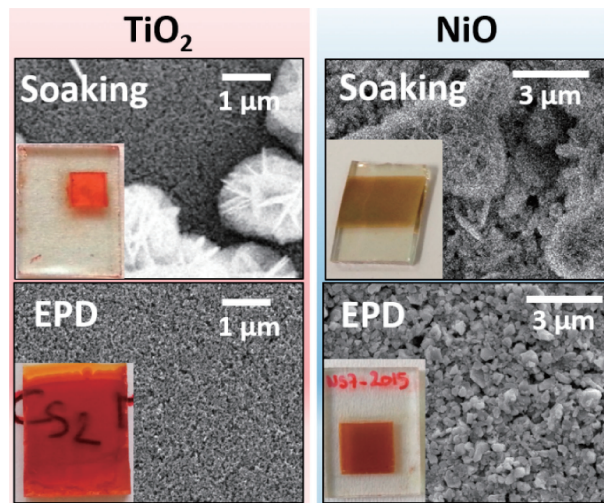
Figure 6. Photographs (the surface of the conductive glass electrodes are 2 cm²) and SEM images of TiO₂ and NiO photoelectrodes surfaces after deposition of cluster **3** by soaking (upper) or EPD method (lower).

Figure 5. (a) The EDX-HRTEM mapping of Cs, Mo and Br elements of the Mo₆ based thin film. (b) XPS spectrum of powder (2) and thin film (2*) based on cluster **2**.

optical properties of the film.[24] The influence of the PDMS on the durability, chemical compatibility and light absorption property of Mo₆ cluster films were characterized by means of field-emission scanning electron microscopy (FE-SEM), energy dispersive spectroscopy (EDS), Fourier transform infrared spectroscopy (FT-IR), and ultraviolet-visible-near infrared (UV-Vis-NIR) spectroscopy. The stabilized PDMS-coated Mo₆ cluster film could be stored for more than 3 years under ambient conditions.

Photovoltaic Properties; Regarding cluster **3**, recently, we investigated their integration on photovoltaic devices as new absorbers in all inorganic solar cells inspired by dye sensitized solar cells (DSSC) and perovskite cells.[85] Indeed, after a preliminary comparison of absorption properties of different molybdenum octahedral clusters in ethanol, it turned out that

the molybdenum iodide cluster (**3**) exhibits a stronger molar absorptivity ranging from UV to the middle of visible. Two types of photoelectrodes, TiO₂-based photoanode for n-DSSC and NiO-based photocathode for p-DSSC, were prepared and tested. In the first processing method, the electrodes were dipped for 48 h in the molecular sensitizer solution to promote the chemisorption. The photoanode and photocathode turned to a persistent red and brown coloration respectively even upon repetitive washings with acetone (Figure 6 upper). It was confirmed by SEM-EDX and HRTEM that this coloration indicated an effective chemisorption of the Mo₆ species on the TiO₂ and NiO electrodes surface. Nevertheless, these analyses confirmed that the Mo₆ coating on the semiconductor surface is not at all homogeneous due to a two step mechanisms: firstly, a homogeneous monolayer of the Mo₆ cluster units is well deposited on the semiconductor surface, but in parallel, an aggregation of the cluster units occurred to form insoluble desert rose-shaped solid state microparticles (Figure 6 upper). In the second processing method, in order to improve the quality of the coating and the transparency of the electrodes, we used EPD as the deposition process of **3** on the TiO₂ or NiO surfaces. As shown in the Figure 6 (lower), we clearly demonstrated that by using EPD process the deposition of film is very much improved. Indeed, the films obtained by EPD have a better absorption and transparency. Their surfaces are very homogeneous and keep the morphology of the initial TiO₂ and NiO coatings. No solid state microparticles are formed. This suggests that the cluster **3** is uniformly chemisorbed on the semiconductor nanoparticles. In all cases, the photoelectrodes were assembled with a counter electrode in platinum and the interspace layer was filled back with an electrolyte. Two different electrolytes were tested: the classical iodide/triiodide couple and the tris(4,4′-di(tert-butyl)-2,2′-bipyridine) cobalt redox couple. The latter gave the best results. It was clearly evidenced that the photoconversion efficiency is much better when we used the EPD as deposition process comparing to the soaking method. Indeed, the open circuit voltage (Voc) of the

TiO$_2$-based cell is improved by 35% whereas the short-circuit current density (Jsc) of the NiO-based cell is almost multiplied by 3. Due to the better homogeneity of the film chemisorption and a decrease of the carrier charge recombination, the V$_{oc}$ and the fill factor of the TiO$_2$-based cell are clearly enhanced (around 35% and 50% respectively) whereas the improvement of the coloration of the NiO-based cell leads to an increase of the Jsc (multiplied by 3). To conclude, the photoconversion efficiency is clearly improved by 35–300%, according to the type of electrolyte or semiconductor used, by using EPD process. In first approximation, this large improvement could be explained by a sufficient generation of compacted and uniform Mo$_6$ thin film with good transparency and controllable thickness thanks to EPD, as already demonstrated for others nanomaterials.[113–115]

Optical Properties; The good morphology of the film was confirmed by optical measurement. Indeed, the UV-Vis absorption spectra exhibited many peaks due to the light interference in the wavelength range from 400 to 2000 nm, showing good homogeneity and transparency of the obtained thin films. The Mo$_6$ coating strongly absorbs light until 450 nm for clusters **2** and **5** and 600 nm for **3** while the ITO glass absorbs NIR light higher than 1100 nm.

Photoluminescent emission (PLE) is another interesting property of the Mo$_6$ cluster and an important parameter to characterize them.[116–119] The PLE of the Mo$_6$ thin film is quite similar to the starting powders and exhibit a very broad emission peak in the red-NIR range. As expected, the luminescence of the cluster **3** is very weak. In the case of the clusters **2** and **5**, the peak positions were centered at 685 nm which is quite close to the value of the powders (for instance the emission of the cluster **2** is centered on 680 nm). Nevertheless, this small change in the PLE spectra could be explained by i) change in the ligand environment, and ii) a higher symmetry of the cluster unit before and after deposition. As a main result, MEK solutions appeared as a good dispersing media for the Mo$_6$ cluster to keep their PL property.

Formation Mechanisms; Based on the variation in the Br/Mo atomic ratios as a function of the applied voltage and deposition time and the modification of the chemical linking observed by FTIR, XPS and TEM, we proposed the following mechanism for the fabrication of the Mo$_6$ cluster film by the EPD process: In the first seconds of the EPD process, highly mobile Br$^-$ anions (originated from OH$^-$ to Br$^-$ ligand substitution in MEK solution) move toward the ITO glass anode in the electric field to form a Br$^-$ rich sublayer. The [Mo$_6$Br$^i_8$-Br$^a_{6-x}$(OH)^a_x]$^{2-}$ cluster units neutralized by H$_3$O$^+$ cations move towards the ITO glass and form (H$_3$O)$_2$[Mo$_6$Br$^i_8$Br$^a_4$(OH)$^a_2$] network.

Due to a lower pH close to the electrode, these later are quickly protonated to form [Mo$_6$Br$^i_8$Br$^a_4$(H$_2$O)$^a_2$] neutral cluster units which interact together to form approximately 6-nm nanoparticles. The outer layers would mostly contain the (H$_3$O)$_2$[Mo$_6$Br$^i_8$Br$^a_4$(OH)$^a_2$] cluster units which are simply packed by the EPD process (high velocity and collision of clusters). In summary, the Mo$_6$ film is a nanocomposite material with a multilayer structure (Figure 7). It is important to note that in the proposed model, the nature of the cations, namely Cs$^+$ or TBA$^+$, of the initial powder precursor does not
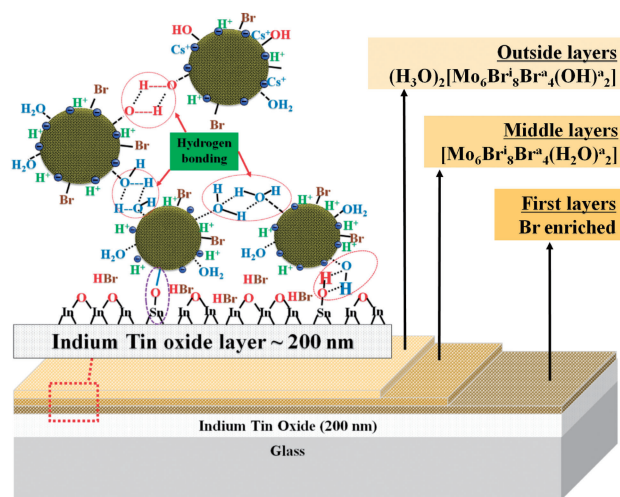

Figure 7. Schematic representation of the multilayered structure of Mo$_6$ cluster thin film.

seem to play a key role at the surface of the electrode. These cations seem to play only an important role in the dissolution of metal cluster in the solvent, and consequently, on the rate of the deposition and thickness. A similar mechanism is expected for cluster **3**. Unfortunately, it was not possible to extract simple and common parameters for all the clusters tested, it seems that each cluster has its own response to the EPD process, or even in some cases, the preparation of transparent thin films is not possible under the conditions we have used. It was the case for the clusters **1**, **4**, **6**, **7** and **8**. It will be discussed in the rest of the article.

Mo$_6$-Polymers Hybrid (1 and 4) Coatings: As described above, the fabrication of thin films based on clusters **1** and **4** without polymer binders was not possible. The understanding of this point is still in progress and will not be discussed in this review article. The clusters **1** and **4** were mixed with different polymers such as PMMA or CAP. Transparent films with a thickness of about 1500 nm were obtained and these films exhibit a strong red photoluminescence emission (Figure 8) even after an exposure to 70% relative humidity and 50 °C for 2 weeks or 4 weeks. The quantum yield values of the nanocomposite film based on PMMA in the excitation wavelength range between 300 and 600 nm is lower than that made with CAP for all different used voltages. Interestingly, the nanocomposite based on CAP prepared at 1 V reached similar quantum yield (15%) to pure cluster **4** in the same condition.

New Nanocomposite Thin Films Based on Nb$_6$ or Ta$_6$ Cluster (6, 7 and 8) for Energy and Environmental Applications. As presented in the introduction, the demand for new, robust, low cost and environmentally-friendly functional transparent thin films for window application is strongly increasing for energy saving applications. Indeed, one of the largest potential energy saving areas may be found in the building, automobile or agriculture sectors due to the use of air conditioning and/or heating systems to regulate indoor temperature. For instance, energy efficient smart glasses or plastic transparent materials could reduce the energy consumption for houses, cars and greenhouses, owing to better thermal insulation by controlling NIR solar radiation.[11–14] The edge-bridged
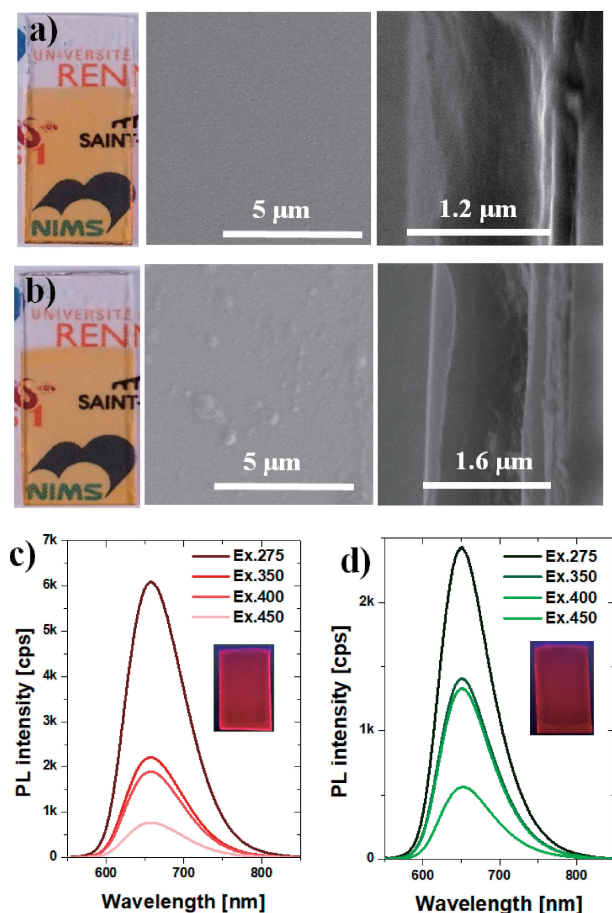
Figure 8. Photographs (size of ITO glass is 1×2 cm), surface morphology and cross section SEM images of deposited films: a) **4**@CAP and b) **4**@PMMA. The photoluminescence of the c) **4**@CAP and d) **4**@PMMA films.

Figure 9. Photographs (size of ITO glass is 1×2 cm), SEM images of surface and the cross section of: a) the brown-**8**@ITO film (25 V and 60 s), and b) the green-**8**@ITO film (20 V and 60 s).

$[M_6L^i_{12}L^a_6]^{n-}$ family of cluster (M = Nb, Ta; $L^{i,a}$ = Cl, Br) appeared as the best candidate thanks to the combination of strong and tunable UV and NIR absorption, and visible transmission (color ranging from green to brown-grey).

Ta_6@PVP@ITO (8) Coating:[13] Initially, we tried to deposit pure Ta_6 clusters (**8**). As shown in Figure 9, brown and green colored films were successfully fabricated by EPD on an ITO coated glass substrate. The best depositions were performed in acetone without water (note brown-**8**@ITO) and with water (note green-**8**@ITO) for the brown and green films respectively. The green-**8**@ITO film was deposited on the cathode (negatively charged) in good agreement with the positive charge of the Ta_6 cluster, whereas surprisingly, the brown-**8**@ITO was formed on the ITO anode side (positively charged) which involved some negatively charged clusters. This latter result is still unclear and we are expecting to propose soon some explanation from TOF-MS experiments realized in collaboration with ILM in Lyon (not shown). Nevertheless, as already known, acetone induced the oxidation of the initial cluster core $[Ta_6Br^i_{12}]^{2+}$ to $[Ta_6Br^i_{12}]^{3+/4+}$ which gives a brown color. We demonstrated that the addition of water (up to a concentration of 0.015 mL of water per mL of acetone) limits the oxidation of the clusters and favors the green color during the 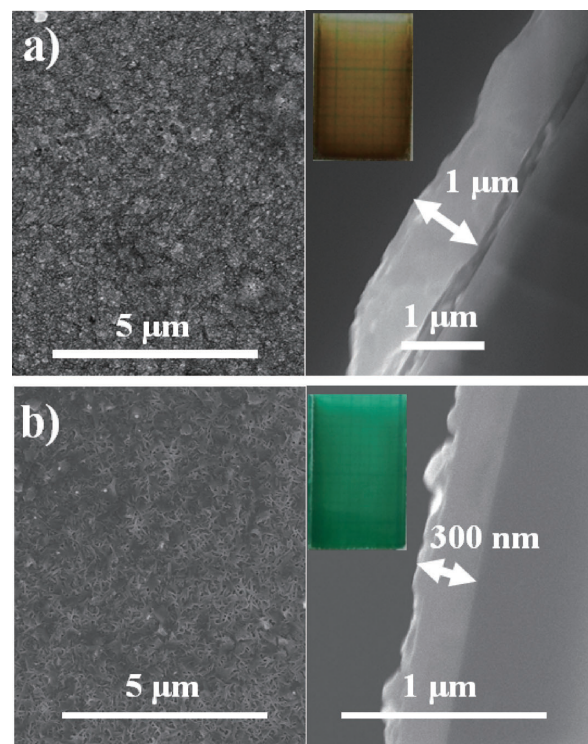EPD process. Indeed, the green color of the films, obtained from the water/acetone solution, clearly suggests that the $[Ta_6Br^i_{12}]^{2+}$ cluster core does not participate in the redox process. The morphology of both films was characterized by SEM investigations. The films have an average thickness of around 500 nm and 300 nm for the brown and green films, respectively, as observed in the SEM images of the cross section of Figures 9a and 9b. Nevertheless, the surface of both films presents some roughness and cracks, and in the case of the green-**8**@ITO film, some agglomerates without well-defined shapes are dispersed on the surface. These agglomerates and high surface roughness favor the scattering of the light and so limits the transmission. During this study, we found that although the water is necessary in acetone to stabilize the green Ta_6 cluster species, it seems to favor particle growth and crystallization which limits the optical properties in the visible range. Grazing incidence X-ray diffraction confirmed this increase in crystallinity of the Ta_6 cluster nanoparticles. Unfortunately, after a few days, while the color of the brown-**8**@ITO film is stable, the green-**8**@ITO films are slightly oxidized by air and loses its green color.

To overcome these negative effects during the deposition process, we investigated the incorporation of a polymer binder, i.e., PVP, into the solution. The purposes of the addition of the polymer were to i) increase the cluster dispersion and limit the Ta_6-based particle growth and the light scattering, and ii) stabilize the green color with time by preventing the oxidation of the clusters. Indeed, it is known that PVP can serve as a surface stabilizer, growth modifier, nanoparticle dispersant, and reducing agent.
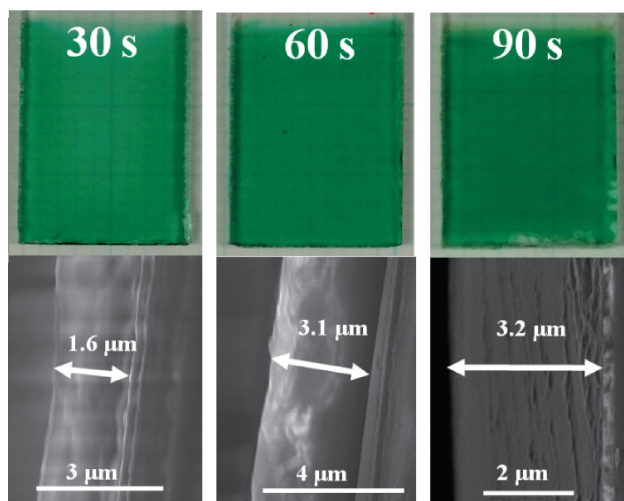
Figure 10. Photographs (size of ITO glass is 1 × 2 cm) and SEM images of the cross section of the **8**@PVP@ITO films prepared at 30 V for 30 s, 60 s and 90 s.
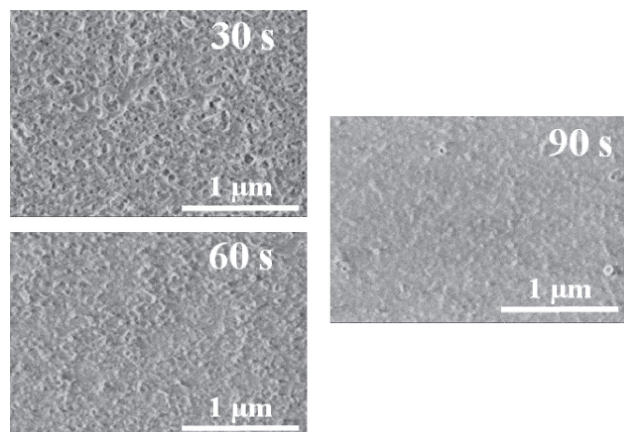

Figure 12. UV-Vis-NIR transmission spectra of the ITO substrate and the **8**@PVP@ITO films obtained at 30 V and 30 s, 60 s and 90 s respectively.

Figure 11. SEM images of the surface of the **8**@PVP@ITO films prepared at 30 V for 30 s, 60 s and 90 s.

Morphology and Structure; After the addition of PVP (weight ratio of Ta_6/PVP = 1), stable, transparent and green films (noted **8**@PVP@ITO) with thickness between 1500 to 3000 nm (film photograph and cross section in Figure 10) were obtained by the EPD process on the cathode side. The optimized applied voltage was estimated at 30 V for the deposition times of 30 s, 60 s or 90 s. The SEM images revealed smooth and homogeneous surfaces (Figure 11). The broad peak observed in the XRD patterns confirmed the amorphous state of the film and a good dispersion of the Ta_6 clusters. This homogeneous dispersion without aggregates over 150 nm was demonstrated by STEM analysis.[8] Similar to the bulk powder, the Raman spectroscopy confirmed the presence of the Ta_6Br_{12} cluster cores in the film.

Optical Properties; As expected, the optical and stability properties of these films were determined to be better than those obtained without the PVP. Indeed, the stability of the green color for the **8**@PVP@ITO films has already surpassed 2 years and their transmittance around 500 nm is greater than that of the green-**8**@ITO films.
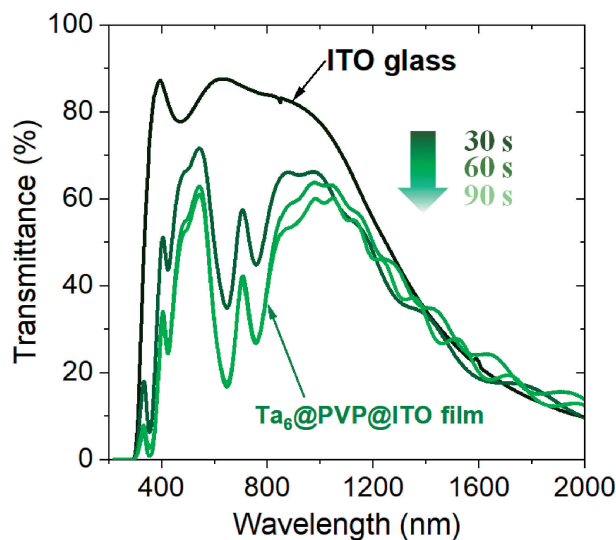
These nanocomposite films exhibited a high transmission in the visible range (Figure 12) which is related to their smooth and homogeneous microstructure. The two absorption peaks in the red around 650 and 750 nm characteristic of the green $[Ta_6Br^i_{12}]^{2+}$ species are much stronger. In order to evaluate the efficiency of the cluster coating as energy saving materials, different figure of merit values, visible transmittance (T_{vis}), solar transmittance (T_{sol}), and T_{vis}/T_{sol} were calculated for the different films.[120–123] T_{sol}, is the integrated spectral transmittance of a window weighted with the normalized solar energy distribution spectrum. T_{vis} was calculated in a similar way, but weighted with the photopic response of the human eye. The T_{vis}/T_{sol} ratio is equal to 1.25 for the best films, such value is a higher energy saving efficiency than most of the inorganic composite coatings reported in the literature.[13] Finally, the resulting green-**8**@PVP@ITO film combined the NIR reflecting properties of the ITO and the UV-red-NIR absorption properties of the clusters.

This study demonstrated that metal atom clusters are new promising UV-NIR blocking pigments which allow i) production of a highly transparent ITO glass with a deep emerald-green color with only a few microns thick coating, and ii) increasing the filtering of the most energetic UV-NIR radiation.

Nb₆@PMMA@ITO (6 and 7) Coatings:[33] In parallel, nanocomposite coatings based on Nb_6 clusters and PMMA were prepared. Similar results were obtained and this gave us the possibility to extend the range of color and mechanical properties. Figure 13 shows photos of successfully prepared homogeneous and transparent coating on ITO substrates. The study of the microstructure by HRTEM revealed a relatively good dispersion of the Nb_6 clusters **6** and **7** into the PMMA. No aggregates with size above 200 nm were observed. As expected, these nanocomposites have the required optical properties, i.e. UV and NIR absorption by combining the Nb_6 and ITO properties respectively. In that cases, the Tvis/Tsol ratios range from 1.07 to 1.19 for **7**@PMMA and **6**@PMMA respectively.
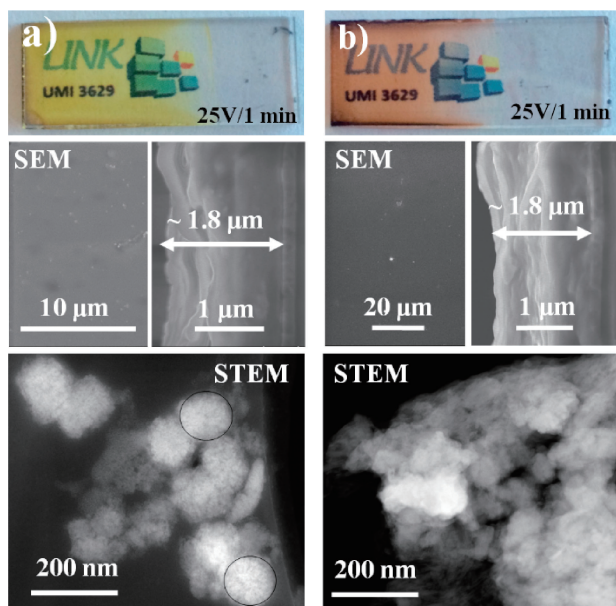
Figure 13. Photographs (size of ITO glass is 1×2 cm) (upper); HR-SEM images of surface morphologies and cross sections (middle); STEM images (lower) of the Nb_6-based cluster anodic films: a) **6**@PMMA, and b) **7**@PMMA.

These ratios could be improved by controlling the oxidation state of the Nb_6 clusters.[33]

4. Conclusion

Keeping in mind the demand for the development of multifunctional inorganic coatings and thin films with high transparency in the visible and tunable UV-NIR absorption, we have demonstrated for the first time that EPD is a very relevant process for the fabrication of new transparent coatings on transparent conductive oxide glass substrate using metal atom clusters as building blocks. EPD is conducted at room temperature under ambient conditions and it has been shown to result in homogeneous and compact cluster (**2**, **3** and **5**) assemblies in a very short time (<90 s), with better physical properties as clearly demonstrated, for instance, for TiO_2 or NiO–based photoelectrodes. Moreover, as proved during this work, some instabilities of the metal clusters (oxidation, quenching of the luminescence, etc.) can be overcome by using a simple polymer as binder during the deposition process. This point was unambiguously verified by adding the PVP to Ta_6 cluster (**8**) or for instance the PMMA with Nb_6 (**6** and **7**) and Mo_6 clusters (**1** and **4**).

Regarding the huge numbers of metal atom clusters available by solid state or soft chemistries, these pioneering works obviously open the door to the development of new transparent functional coatings in complement of other chemical solution deposition techniques.[124–128] Indeed, after the dissolution of the solid state precursors in the appropriate solvent and the establishment of the best deposition parameters (i.e. solvent, concentration, applied voltage, time, etc.) which seem different for each cluster unit, metal atom clusters appeared to be versatile building blocks that could exhibit a broad range of specific properties (catalytic, optical, transport, etc.). In this work,

thanks to some of these properties, it was possible to combine specific absorption in UV and/or NIR, or luminescence properties with high transparency in the visible. To conclude, the work presented here can be extended in several directions (large area, flexible or rough substrate, etc.) and we believe that the electrophoretic deposition of metal atom clusters is a new field of research with wide a range of potential applications (optoelectronic, sensor, catalysis, etc.).

To enlarge perspective, the use of metal clusters as nanoprobes (redox, luminescence…) in specific media is expected to provide information otherwise difficult to gather by using other physicochemical approaches.[129]

References

1 http://www.marketsandmarkets.com/PressReleases/thin-film-material.asp.

2 H. Kataoka, T. Nakanishi, S. Omagari, Y. Takabatake, Y. Kitagawa, Y. Hasegawa, *Bull. Chem. Soc. Jpn.* **2016**, *89*, 103.

3 K. Inoue, *Bull. Chem. Soc. Jpn.* **2016**, *89*, 1416.

4 Y. Tobe, K. Tahara, S. De Feyter, *Bull. Chem. Soc. Jpn.* **2016**, *89*, 1277.

5 H.-W. Chen, C.-Y. Hong, C.-W. Kung, C.-Y. Mou, K. C.-W. Wu, K.-C. Ho, *J. Power Sources* **2015**, *288*, 221.

6 H.-W. Chen, Y.-T. Liao, J.-G. Chen, K.-C. W. Wu, K.-C. Ho, *J. Mater. Chem.* **2011**, *21*, 17511.

7 A.-L. Anderson, S. Chen, L. Romero, I. Top, R. Binions, *Buildings* **2016**, *6*, 37.

8 F. Meinardi, S. Ehrenberg, L. Dhamo, F. Carulli, M. Mauri, F. Bruni, R. Simonutti, U. Kortshagen, S. Brovelli, *Nat. Photonics* **2017**, *11*, 177.

9 C. J. Traverse, R. Pandey, M. C. Barr, R. R. Lunt, *Nat. Energy* **2017**, *2*, 849.

10 R. Baetens, B. P. Jelle, A. Gustavsen, *Sol. Energy Mater. Sol. Cells* **2010**, *94*, 87.

11   A. Llordés, G. Garcia, J. Gazquez, D. J. Milliron, *Nature* **2013**, *500*, 323.

12   C. G. Granqvist, *Thin Solid Films* **2014**, *564*, 1.

13   T. K. N. Nguyen, A. Renaud, M. Wilmet, N. Dumait, S. Paofai, B. Dierre, W. Chen, N. Ohashi, S. Cordier, F. Grasset, T. Uchikoshi, *J. Mater. Chem. C* **2017**, *5*, 10477.

14   L. V. Besteiro, X.-T. Kong, Z. Wang, F. Rosei, A. O. Govorov, *Nano Lett.* **2018**, *18*, 3147.

15   Y. Sakka, T. Uchikoshi, *KONA Powder Part. J.* **2010**, *28*, 74.

16   B. Ferrari, R. Moreno, *J. Eur. Ceram. Soc.* **2010**, *30*, 1069.

17   A. R. Boccaccini, J. H. Dickerson, *J. Phys. Chem. B* **2013**, *117*, 1501.

18   A. J. Pascall, F. Qian, G. Wang, M. A. Worsley, Y. Li, J. D. Kuntz, *Adv. Mater.* **2014**, *26*, 2252.

19   M. Diba, D. W. H. Fam, A. R. Boccaccini, M. S. P. Shaffer, *Prog. Mater. Sci.* **2016**, *82*, 83.

20   M. S. Nam, U. Patil, B. Park, H. B. Sim, S. C. Jun, *RSC Adv.* **2016**, *6*, 101592.

21   H.-W. Tsai, C.-W. Chen, S. R. Thomas, C.-H. Hsu, W.-C. Tsai, Y.-Z. Chen, Y.-C. Wang, Z. M. Wang, H.-F. Hong, Y.-L. Chueh, *Sci. Rep.* **2016**, *6*, 19102.

22   J. B. Talbot, J. McKittrick, *ECS J. Solid State Sci. Technol.* **2016**, *5*, R3107.

23   O. Černohorský, J. Grym, R. Yatskiv, V. H. Pham, J. H. Dickerson, *ACS Appl. Mater. Interfaces* **2016**, *8*, 19680.

24   S. Tokunaga, Y. Itoh, Y. Yaguchi, H. Tanaka, F. Araoka, H. Takezoe, T. Aida, *Adv. Mater.* **2016**, *28*, 4077.

25   K. Katagiri, Y. Tanaka, K. Uemura, K. Inumaru, T. Seki, Y. Takeoka, *NPG Asia Mater.* **2017**, *9*, e355.

26   P. Collini, S. Kota, A. D. Dillon, M. W. Barsoum, A. T. Fafarman, *J. Electrochem. Soc.* **2017**, *164*, D573.

27   B. Giera, L. A. Zepeda-Ruiz, A. J. Pascall, T. H. Weisgraber, *Langmuir* **2017**, *33*, 652.

28   J. Han, E. Lee, J. K. Dudoff, M. Bagge-Hansen, J. R. I. Lee, A. J. Pascall, J. D. Kuntz, T. M. Willey, M. A. Worsley, T. Y.-J. Han, *Adv. Opt. Mater.* **2017**, *5*, 1600838.

29   http://www.nims.go.jp/eng/collaboration/hdfqf10000083jv1.html.

30   T. K. N. Nguyen, F. Grasset, B. Dierre, C. Matsunaga, S. Cordier, P. Lemoine, N. Ohashi, T. Uchikoshi, *ECS J. Solid State Sci. Technol.* **2016**, *5*, R178.

31   T. K. N. Nguyen, B. Dierre, F. Grasset, A. Renaud, S. Cordier, P. Lemoine, N. Ohashi, T. Uchikoshi, *J. Electrochem. Soc.* **2017**, *164*, D412.

32   T. K. N. Nguyen, B. Dierre, F. Grasset, N. Dumait, S. Cordier, P. Lemoine, A. Renaud, H. Fudouzi, N. Ohashi, T. Uchikoshi, *Coatings* **2017**, *7*, 114.

33   N. T. K. Nguyen, M. Dubernet, M. Wilmet, F. Grasset, N. Shirahata, G. Ridzek, N. Dumait, M. Amela-Cortes, A. Renaud, S. Cordier, Y. Molard, T. Uchikoshi, *R. Soc. Open Sci.*, submitted.

34   M. Potel, C. Perrin, A. Perrin, M. Sergent, *Mater. Res. Bull.* **1986**, *21*, 1239.

35   K. Kirakci, S. Cordier, C. Perrin, *Z. Anorg. Allg. Chem.* **2005**, *631*, 411.

36   M. Amela-Cortes, S. Paofai, S. Cordier, H. Folliot, Y. Molard, *Chem. Commun.* **2015**, *51*, 8177.

37   P. B. Fleming, L. A. Mueller, R. E. McCarley, *Inorg. Chem.* **1967**, *6*, 1.

38   A. Simon, H.-G. von Schnering, H. Schäfer, *Z. Anorg. Allg. Chem.* **1968**, *361*, 235.

39   F. W. Koknat, J. A. Parsons, A. Vongvusharintra, *Inorg. Chem.* **1974**, *13*, 1699.

40   P. Amrollahi, J. S. Krasinski, R. Vaidyanathan, L. Tayebi, D. Vashaee, in *Handbook of Nanoelectrochemistry*, Springer, Cham, **2016**, p. 561. doi:10.1007/978-3-319-15266-0_7.

41   H. C. Hamaker, E. J. W. Verwey, *Trans. Faraday Soc.* **1940**, *35*, 180.

42   N. Koura, T. Tsukamoto, H. Shoji, T. Hotta, *Jpn. J. Appl. Phys.* **1995**, *34*, 1643.

43   P. Sarkar, P. S. Nicholson, *J. Am. Ceram. Soc.* **1996**, *79*, 1987.

44   Y. Fukada, N. Nagarajan, W. Mekky, Y. Bao, H.-S. Kim, P. S. Nicholson, *J. Mater. Sci.* **2004**, *39*, 787.

45   L. Besra, M. Liu, *Prog. Mater. Sci.* **2007**, *52*, 1.

46   J. J. Van Tassel, C. A. Randall, *Key Eng. Mater.* **2006**, *314*, 167.

47   I. Corni, M. P. Ryan, A. R. Boccaccini, *J. Eur. Ceram. Soc.* **2008**, *28*, 1353.

48   M. Ammam, *RSC Adv.* **2012**, *2*, 7633.

49   A. Chávez-Valdez, A. R. Boccaccini, *Electrochim. Acta* **2012**, *65*, 70.

50   F. Keller, H. Nirschl, W. Dörfler, E. Woldt, *J. Eur. Ceram. Soc.* **2015**, *35*, 2619.

51   I. Zhitomirsky, L. Gal-Or, *J. Mater. Sci.: Mater. Med.* **1997**, *8*, 213.

52   M. Wei, A. J. Ruys, B. K. Milthorpe, C. C. Sorrell, *J. Biomed. Mater. Res.* **1999**, *45*, 11.

53   M. Holgado, F. García-Santamaría, A. Blanco, M. Ibisate, A. Cintas, H. Míguez, C. J. Serna, C. Molpeceres, J. Requena, A. Mifsud, F. Meseguer, C. López, *Langmuir* **1999**, *15*, 4701.

54   B. Gao, G. Z. Yue, Q. Qiu, Y. Cheng, H. Shimoda, L. Fleming, O. Zhou, *Adv. Mater.* **2001**, *13*, 1770.

55   A. R. Boccaccini, J. Cho, J. A. Roether, B. J. C. Thomas, E. J. Minay, M. S. P. Shaffer, *Carbon* **2006**, *44*, 3149.

56   J. Cho, K. Konopka, K. Rożniatowski, E. García-Lecina, M. S. P. Shaffer, A. R. Boccaccini, *Carbon* **2009**, *47*, 58.

57   Z.-S. Wu, S. Pei, W. Ren, D. Tang, L. Gao, B. Liu, F. Li, C. Liu, H.-M. Cheng, *Adv. Mater.* **2009**, *21*, 1756.

58   G. Anné, K. Vanmeensel, J. Vleugels, O. Van der Biest, *Colloids Surf., A* **2004**, *245*, 35.

59   S. Dor, S. Rühle, A. Ofir, M. Adler, L. Grinis, A. Zaban, *Colloids Surf., A* **2009**, *342*, 70.

60   D. Hanaor, M. Michelazzi, P. Veronesi, C. Leonelli, M. Romagnoli, C. Sorrell, *J. Eur. Ceram. Soc.* **2011**, *31*, 1041.

61   R. Kawakami, T. Yuasa, K. Ito, Y. Sato, Y. Mori, M. Adachi, S. Yoshikado, *J. Aust. Ceram. Soc.* **2012**, *48*, 236.

62   L. A. Ma, T. L. Guo, *Ceram. Int.* **2013**, *39*, 6923.

63   Y. Huang, D. K. Sarkar, X.-G. Chen, *Appl. Surf. Sci.* **2015**, *327*, 327.

64   S. N. Hosseini, H. Salimi Jazi, M. H. Fathi, *Mater. Lett.* **2015**, *143*, 16.

65   H. Zhu, H. Liu, I. Zhitomirsky, S. Zhu, *Mater. Lett.* **2015**, *142*, 19.

66   I. Hod, W. Bury, D. M. Karlin, P. Deria, C.-W. Kung, M. J. Katz, M. So, B. Klahr, D. Jin, Y.-W. Chung, T. W. Odom, O. K. Farha, J. T. Hupp, *Adv. Mater.* **2014**, *26*, 6295.

67   C. Streich, S. Koenen, M. Lelle, K. Peneva, S. Barcikowski, *Appl. Surf. Sci.* **2015**, *348*, 92.

68   J. Liu, Z. Wu, T. Li, D. Zhou, K. Zhang, Y. Sheng, J. Cui, H. Zhang, B. Yang, *Nanoscale* **2016**, *8*, 395.

69   A. Perrin, C. Perrin, *C. R. Chim.* **2012**, *15*, 815.

70   V. Fedorov, *J. Cluster Sci.* **2015**, *26*, 3.

71   R. Chevrel, M. Sergent, J. Prigent, *J. Solid State Chem.*

1971, *3*, 515.

72   D. Aurbach, Z. Lu, A. Schechter, Y. Gofer, H. Gizbar, R. Turgeman, Y. Cohen, M. Moshkovich, E. Levi, *Nature* **2000**, *407*, 724.

73   D. Aurbach, G. S. Suresh, E. Levi, A. Mitelman, O. Mizrahi, O. Chusid, M. Brunelli, *Adv. Mater.* **2007**, *19*, 4260.

74   D. Dybtsev, C. Serre, B. Schmitz, B. Panella, M. Hirscher, M. Latroche, P. L. Llewellyn, S. Cordier, Y. Molard, M. Haouas, F. Taulelle, G. Férey, *Langmuir* **2010**, *26*, 11283.

75   P. Gougeon, P. Gall, R. Al Rahal Al Orabi, B. Fontaine, R. Gautier, M. Potel, T. Zhou, B. Lenoir, M. Colin, C. Candolfi, A. Dauscher, *Chem. Mater.* **2012**, *24*, 2899.

76   S. Fujii, T. Horiguchi, S. Akagi, N. Kitamura, *Inorg. Chem.* **2016**, *55*, 10259.

77   S. Cordier, F. Grasset, Y. Molard, M. Amela-Cortes, R. Boukherroub, S. Ravaine, M. Mortier, N. Ohashi, N. Saito, H. Haneda, *J. Inorg. Organomet. Polym.* **2015**, *25*, 189.

78   P. S. Kuttipillai, Y. Zhao, C. J. Traverse, R. J. Staples, B. G. Levine, R. R. Lunt, *Adv. Mater.* **2016**, *28*, 320.

79   Y. Molard, *Acc. Chem. Res.* **2016**, *49*, 1514.

80   R. R. Lunt, P. S. Kuttipillai, United States patent US 2015/0069366 A1, 2015 Mar 12.

81   M. Prévôt, M. Amela-Cortes, S. K. Manna, R. Lefort, S. Cordier, H. Folliot, L. Dupont, Y. Molard, *Adv. Funct. Mater.* **2015**, *25*, 4966.

82   J. Bigeon, N. Huby, M. Amela-Cortes, Y. Molard, A. Garreau, S. Cordier, B. Bêche, J.-L. Duvail, *Nanotechnology* **2016**, *27*, 255201.

83   Y. Zhao, R. R. Lunt, *Adv. Energy Mater.* **2013**, *3*, 1143.

84   Y. Zhao, G. A. Meek, B. G. Levine, R. R. Lunt, *Adv. Opt. Mater.* **2014**, *2*, 606.

85   A. Renaud, F. Grasset, B. Dierre, T. Uchikoshi, N. Ohashi, T. Takei, A. Planchat, L. Cario, S. Jobic, F. Odobel, S. Cordier, *ChemistrySelect* **2016**, *1*, 2284.

86   S. Kamiguchi, S. Takaku, M. Kodomari, T. Chihara, *J. Mol. Catal. A: Chem.* **2006**, *260*, 43.

87   A. Barras, S. Cordier, R. Boukherroub, *Appl. Catal., B* **2012**, *123–124*, 1; S. Kamiguchi, K. Takeda, R. Kajio, K. Okumura, S. Nagashima, T. Chihara, *J. Cluster Sci.* **2013**, *24*, 559.

88   S. Nagashima, K. Kudo, H. Yamazaki, S. Kamiguchi, T. Chihara, *Appl. Catal., A* **2013**, *450*, 50.

89   A. Barras, M. R. Das, R. R. Devarapalli, M. V. Shelke, S. Cordier, S. Szunerits, R. Boukherroub, *Appl. Catal., B* **2013**, *130–131*, 270.

90   P. Kumar, H. P. Mungse, S. Cordier, R. Boukherroub, O. P. Khatri, S. L. Jain, *Carbon* **2015**, *94*, 91.

91   J. Löwe, D. Stock, B. Jap, P. Zwickl, W. Baumeister, R. Huber, *Science* **1995**, *268*, 533.

92   P. Cramer, D. A. Bushnell, J. Fu, A. L. Gnatt, B. Maier-Davis, N. E. Thompson, R. R. Burgess, A. M. Edwards, P. R. David, R. D. Kornberg, *Science* **2000**, *288*, 640.

93   K. N. Ferreira, T. M. Iverson, K. Maghlaoui, J. Barber, S. Iwata, *Science* **2004**, *303*, 1831.

94   F. Grasset, F. Dorson, S. Cordier, Y. Molard, C. Perrin, A.-M. Marie, T. Sasaki, H. Haneda, Y. Bando, M. Mortier, *Adv. Mater.* **2008**, *20*, 143.

95   F. Grasset, F. Dorson, Y. Molard, S. Cordier, V. Demange, C. Perrin, V. Marchi-Artzner, H. Haneda, *Chem. Commun.* **2008**, 4729.

96   T. Aubert, F. Cabello-Hurtado, M.-A. Esnault, C. Neaime, D. Lebret-Chauvel, S. Jeanne, P. Pellen, C. Roiland, L. Le Polles, N. Saito, K. Kimoto, H. Haneda, N. Ohashi, F. Grasset, S. Cordier,

97   N. Nerambourg, T. Aubert, C. Neaime, S. Cordier, M. Mortier, G. Patriarche, F. Grasset, *J. Colloid Interface Sci.* **2014**, *424*, 132.

98   K. Kirakci, V. Šícha, J. Holub, P. Kubát, K. Lang, *Inorg. Chem.* **2014**, *53*, 13012.

99   K. Kirakci, P. Kubát, K. Fejfarová, J. Martinčík, M. Nikl, K. Lang, *Inorg. Chem.* **2016**, *55*, 803.

100   K. Kirakci, P. Kubát, M. Kučeráková, V. Šícha, H. Gbelcová, P. Lovecká, P. Grznárová, T. Ruml, K. Lang, *Inorg. Chim. Acta* **2016**, *441*, 42.

101   A. O. Solovieva, Y. A. Vorotnikov, K. E. Trifonova, O. A. Efremova, A. A. Krasilnikova, K. A. Brylev, E. V. Vorontsova, P. A. Avrorov, L. V. Shestopalova, A. F. Poveshchenko, Y. V. Mironov, M. A. Shestopalov, *J. Mater. Chem. B* **2016**, *4*, 4839.

102   C. Neaime, M. Amela-Cortes, F. Grasset, Y. Molard, S. Cordier, B. Dierre, M. Mortier, T. Takei, K. Takahashi, H. Haneda, M. Verelst, S. Lechevallier, *Phys. Chem. Chem. Phys.* **2016**, *18*, 30166.

103   N. A. Vorotnikova, O. A. Efremova, A. R. Tsygankova, K. A. Brylev, M. V. Edeleva, O. G. Kurskaya, A. J. Sutherland, A. M. Shestopalov, Y. V. Mironov, M. A. Shestopalov, *Polym. Adv. Technol.* **2016**, *27*, 922.

104   A. Beltrán, M. Mikhailov, M. N. Sokolov, V. Pérez-Laguna, A. Rezusta, M. José Revillo, F. Galindo, *J. Mater. Chem. B* **2016**, *4*, 5975.

105   F. Cabello-Hurtado, M. D. Lozano-Baena, C. Neaime, A. Burel, S. Jeanne, P. Pellen-Mussi, S. Cordier, F. Grasset, *J. Nanopart. Res.* **2016**, *18*, 69.

106   Y. A. Vorotnikov, O. A. Efremova, N. A. Vorotnikova, K. A. Brylev, M. V. Edeleva, A. R. Tsygankova, A. I. Smolentsev, N. Kitamura, Y. V. Mironov, M. A. Shestopalov, *RSC Adv.* **2016**, *6*, 43367.

107   E. V. Svezhentseva, A. O. Solovieva, Y. A. Vorotnikov, O. G. Kurskaya, K. A. Brylev, A. R. Tsygankova, M. V. Edeleva, S. N. Gyrylova, N. Kitamura, O. A. Efremova, M. A. Shestopalov, Y. V. Mironov, A. M. Shestopalov, *New J. Chem.* **2017**, *41*, 1670.

108   J.-F. Dechézelles, T. Aubert, F. Grasset, S. Cordier, C. Barthou, C. Schwob, A. Maître, R. A. L. Vallée, H. Cramail, S. Ravaine, *Phys. Chem. Chem. Phys.* **2010**, *12*, 11993.

109   T. Aubert, N. Nerambourg, N. Saito, H. Haneda, N. Ohashi, M. Mortier, S. Cordier, F. Grasset, *Part. Part. Syst. Charact.* **2013**, *30*, 90.

110   T. G. Truong, B. Dierre, F. Grasset, N. Saito, N. Saito, T. K. N. Nguyen, K. Takahashi, T. Uchikoshi, M. Amela-Cortes, Y. Molard, S. Cordier, N. Ohashi, *Sci. Technol. Adv. Mater.* **2016**, *17*, 443.

111   L. J. Guggenberger, A. W. Sleight, *Inorg. Chem.* **1969**, *8*, 2041.

112   Y.-Q. Zheng, Y. Grin, H. G. von Schnering, *Z. Kristallogr. NCS* **1998**, *213*, 469.

113   S. Bai, S. He, Y. Jin, Z. Wu, Z. Xia, B. Sun, X. Wang, Z. Ye, F. Gao, S. Shao, F. Zhang, *RSC Adv.* **2015**, *5*, 8216.

114   O. O. Otelaja, D.-H. Ha, T. Ly, H. Zhang, R. D. Robinson, *ACS Appl. Mater. Interfaces* **2014**, *6*, 18911.

115   Y. Kosuge, Y. Iso, T. Isobe, *Langmuir* **2018**, *34*, 3813.

116   A. W. Maverick, H. B. Gray, *J. Am. Chem. Soc.* **1981**, *103*, 1298.

117   B. Dierre, K. Costuas, N. Dumait, S. Paofai, M. Amela-Cortes, Y. Molard, F. Grasset, Y. Cho, K. Takahashi, N. Ohashi, T. Uchikoshi, S. Cordier, *Sci. Technol. Adv. Mater.* **2017**, *18*, 458.

118   N. Saito, P. Lemoine, S. Cordier, Y. Wada, T. Ohsawa, N.

Saito, F. Grasset, J. S. Cross, N. Ohashi, *CrystEngComm* **2017**, *19*, 6028.

119   S. Akagi, S. Fujii, N. Kitamura, *Dalton Trans.* **2018**, *47*, 1131.

120   G. B. Smith, C. A. Deller, P. D. Swift, A. Gentle, P. D. Garrett, W. K. Fisher, *J. Nanopart. Res.* **2002**, *4*, 157.

121   S. Schelm, G. B. Smith, P. D. Garrett, W. K. Fisher, *J. Appl. Phys.* **2005**, *97*, 124314.

122   N. L. Stokes, J. A. Edgar, A. M. McDonagh, M. B. Cortie, *J. Nanopart. Res.* **2010**, *12*, 2821.

123   M. Carboni, M. Carravetta, X. L. Zhang, E. Stulz, *J. Mater. Chem. C* **2016**, *4*, 1584.

124   G. Decher, *Science* **1997**, *277*, 1232.

125   D. Grosso, F. Cagnol, G. Soler-Illia, E. L. Crepaldi, H. Amenitsch, A. Brunet-Bruneau, A. Bourgeois, C. Sanchez, *Adv. Funct. Mater.* **2004**, *14*, 309.

126   K. Ariga, Q. Ji, J. P. Hill, Y. Bando, M. Aono, *NPG Asia Mater.* **2012**, *4*, e17.

127   S. J. Kim, S. Yoon, H. J. Kim, *Jpn. J. Appl. Phys.* **2014**, *53*, 02BA02.

128   M. Komiyama, T. Mori, K. Ariga, *Bull. Chem. Soc. Jpn.* **2018**, *91*, 1075.

129   S. Antonello, F. Maran, *Curr. Opin. Electrochem.* **2017**, *2*, 18.